Antitumor Activity of GSK1904529A, a Small-molecule Inhibitor of the Insulin-like Growth Factor-I Receptor Tyrosine Kinase

Peter Sabbatini,[1] Jason L. Rowand,[1] Arthur Groy,[1] Susan Korenchuk,[1] Qi Liu,[1] Charity Atkins,[1] Melissa Dumble,[1] Jingsong Yang,[1] Kelly Anderson,[1] Brian J. Wilson,[2] Kyle A. Emmitte,[2] Sridhar K. Rabindran,[1] and Rakesh Kumar[1]

Abstract

Purpose: Dysregulation of the insulin-like growth factor-I receptor (IGF-IR) signaling pathway has been implicated in the development of many types of tumors, including prostate, colon, breast, pancreatic, ovarian, and sarcomas. Agents that inhibit IGF-IR activity may be useful in treatment of patients with various cancers.

Experimental Design: Kinase assays were used to identify a selective small-molecule inhibitor of IGF-IR activity. The effects of this compound on IGF-IR signaling, cell proliferation, and the cell cycle were determined using a panel of cell lines. Antitumor activity was evaluated in human tumor xenografts growing in athymic mice. Inhibition of IGF-IR and the closely related insulin receptor (IR) was measured *in vivo*, and the effect on glucose metabolism was evaluated.

Results: GSK1904529A selectively inhibits IGF-IR and IR with IC_{50}s of 27 and 25 nmol/L, respectively. GSK1904529A blocks receptor autophosphorylation and downstream signaling, leading to cell cycle arrest. It inhibits the proliferation of cell lines derived from solid and hematologic malignancies, with multiple myeloma and Ewing's sarcoma cell lines being most sensitive. Oral administration of GSK1904529A decreases the growth of human tumor xenografts in mice, consistent with a reduction of IGF-IR phosphorylation in tumors. Despite the potent inhibitory activity of GSK1904529A on IR *in vitro* and *in vivo*, minimal effects on blood glucose levels are observed in animals at doses that show significant antitumor activity.

Conclusion: GSK1904529A is a promising candidate for therapeutic use in IGF-IR – dependent tumors.

The insulin-like growth factor-I receptor (IGF-IR) belongs to the insulin receptor (IR) family of receptor tyrosine kinases, which regulates diverse cellular functions, such as proliferation, survival, differentiation, and motility (1, 2). On binding to its ligands, IGF-I and IGF-II, the receptor undergoes autophosphorylation within the activation loop of the kinase, inducing conformational changes that lead to enzyme activation. Docking proteins bind to the phosphorylated sites in the cytoplasmic domain of the activated receptor, leading to initiation of a signal transduction cascade. The phosphatidylinositol 3-kinase (PI3K)/AKT and mitogen-activated protein kinase (MAPK) pathways are the major signaling pathways through which IGF-IR exerts its cellular effects. Activity of IGF-IR is also regulated by levels of binding proteins, IGFBP1-7, which bind and sequester the ligands, preventing them from activating the receptor (1).

Several lines of evidence support the role of IGF-IR in tumorigenesis. IGF-IR is required for transformation of mouse embryonic fibroblasts by oncogenes and inhibition of IGF-IR signaling using various approaches (e.g., antibodies, antisense, IGF binding proteins, small interfering RNA, and dominant-negative receptors) results in decreased proliferation and survival of tumor cells *in vitro* and *in vivo* (1, 3 – 5). In animal tumor models, low IGF-I levels in IGF-I – deficient mice are associated with reduced growth of tumor xenografts and increased resistance to carcinogen-induced tumorigenesis. Conversely, overexpression or expression of a constitutively active receptor in transgenic animal models leads to increased tumorigenesis as well as increased tumor invasiveness (6). In human studies, the IGF-IR signaling pathway is activated in many cancers, including prostate, colon, breast, pancreatic, liver, and ovarian cancers and sarcomas, due to aberrant expression of IGF-IR or its ligands and/or by decreased levels of the binding proteins (2, 7). These data suggest that the IGF-IR pathway plays a significant role in tumorigenesis, and inhibition of this pathway is a viable anticancer strategy. In fact, several antibodies and small-molecule kinase inhibitors targeting IGF-IR are in preclinical and clinical development (2, 8). Early trials with IGF-IR antibodies have shown clinical benefit in patients with multiple myeloma (9) and sarcoma (10) when used as a single agent and in patients with non – small cell lung cancer in combination with

Authors' Affiliations: [1]GlaxoSmithKline, Oncology R&D, Collegeville, Pennsylvania and [2]GlaxoSmithKline, Oncology R&D, Research Triangle Park, North Carolina

Received 10/1/08; revised 1/23/09; accepted 1/27/09; published OnlineFirst 4/21/09. The costs of publication of this article were defrayed in part by the payment of page charges. This article must therefore be hereby marked *advertisement* in accordance with 18 U.S.C. Section 1734 solely to indicate this fact.

Requests for reprints: Rakesh Kumar, GlaxoSmithKline, Oncology R&D, 1250 South Collegeville Road, Collegeville, PA 19426. Phone: 610-917-4855; Fax: 610-917-4181; E-mail: rakesh.2.kumar@gsk.com.

doi:10.1158/1078-0432.CCR-08-2530

Translational Relevance

The insulin-like growth factor-I receptor (IGF-IR) regulates diverse cellular functions, such as proliferation, survival, differentiation, and motility. Several lines of evidence *in vitro*, in animal models, and in early human clinical trials with IGF-IR antibodies have provided strong validation of IGF-IR as a therapeutic target for cancer. The small-molecule kinase inhibitor GSK1904529A is a promising candidate for therapeutic use in solid and hematologic cancers based on its *in vitro* activity and antitumor effects in tumor xenograft models at well-tolerated doses. Clinical benefits of IGF-IR inhibitors are predicted in patients with IGF-I – dependent tumors as a single agent or in combination with other targeted or cytotoxic therapy.

chemotherapy (11). These studies provide a strong clinical validation of IGF-IR as a therapeutic target for cancer. Furthermore, IGF-IR activation has been associated with resistance to targeted agents such as trastuzumab in breast cancer (12, 13) and inhibition of IGF-IR signaling may reverse resistance to these agents.

We describe here the characteristics of a small-molecule kinase inhibitor, GSK1904529A, which potently inhibits IGF-IR and IR activities *in vitro* and *in vivo*. We profile its antiproliferative effects in cell lines derived from solid and hematologic malignancies and describe its antitumor activity in tumor xenografts.

Materials and Methods

GSK1904529A. GSK1904529A was synthesized at GlaxoSmithKline (Supplementary Fig. S1). For *in vitro* studies, GSK1904529A was dissolved in DMSO at 10 mmol/L. For *in vivo* studies, GSK1904529A was formulated in 20% sulfobutylether-β-cyclodextrin (pH 3.5; ISP).

Animals. Female athymic *nu/nu* CD-1 mice were obtained from Charles River. Animal studies were done in compliance with federal requirements, GlaxoSmithKline policy on the Care and Use of Animals, and related codes of practice.

Kinase assays. Baculovirus-expressed glutathione *S*-transferase – tagged proteins encoding the intracellular domain of IGF-IR (amino acids 957-1367) and IR (amino acids 979-1382) were used for determination of IC_{50}s. Kinases were activated by preincubating the enzyme (2.7 μmol/L final concentration) in 50 mmol/L HEPES (pH 7.5), 10 mmol/L $MgCl_2$, 0.1 mg/mL bovine serum albumin, and 2 mmol/L ATP (all chemical reagents from Sigma-Aldrich unless otherwise noted). Compounds were diluted in DMSO and dispensed into the assay plates (100 nL/well). Kinase reactions contained (in 10 μL volume) 50 mmol/L HEPES (pH 7.5), 3 mmol/L DTT, 0.1 mg/mL bovine serum albumin, 1 mmol/L CHAPS, 10 mmol/L $MgCl_2$, 10 μmol/L ATP, 500 nmol/L substrate peptide (biotin-aminohexyl-AEEEEYMMMMAKKKK-NH_2; QPC), and 0.5 nmol/L activated enzyme. Reactions were stopped after 1 h at room temperature with 33 μmol/L EDTA. Peptide phosphorylation was measured by time-resolved fluorescence resonance energy transfer with 7 nmol/L streptavidin-Surelight allophycocyanin (Perkin-Elmer) and 1 nmol/L europium-conjugated phosphotyrosine antibodies (Perkin-Elmer). Plates were read in a Victor X5 or ViewLux 1430 ultra HTS microplate imager (Perkin-Elmer).

A filter binding assay was used for $^{app}K_i$ determinations. IGF-IR and IR kinase domains were activated by preincubating at 500 nmol/L in assay buffer A [50 mmol/L HEPES (pH 7.2), 10 mmol/L $MgCl_2$, 0.2 mg/mL bovine serum albumin, 1× phosphatase inhibitor cocktail II (Sigma-Aldrich)] with 1 mmol/L ATP for 30 min. Reactions contained (in 40 μL) 0.5 nmol/L activated enzyme, 40 μmol/L ATP (Teknova), and 7.5 μmol/L peptide substrate ($1 \times K_m$ and $1.5 \times K_m$ concentration, respectively, for both IGF-IR and IR; 21st Century Biochemicals) and [γ-^{33}P]ATP (100-500 cpm/pmol, 10 mCi/mL in 10 mmol/L Tricine; Perkin-Elmer). The peptide substrate had the same sequence as that used for the time-resolved fluorescence assay but without the biotin moiety. Inhibitor dilutions were prepared in DMSO and dispensed (1 μL/well) into the wells of a 96-well, half-area nonbinding surface plates (Corning). The enzyme mix was added and incubated with inhibitor for 6 h to allow the inhibitor-enzyme binding to reach equilibrium. Reactions were initiated by the addition of the reaction mix containing ATP and peptide substrate. The reactions were quenched after 120 min, filtered through MAPHN0B50 filter plates (Millipore Corp.), and washed, and the product was quantified by liquid scintillation counting using MicroScint-20 (Perkin-Elmer) in a MicroBeta-1450 plate reader (Perkin-Elmer). IC_{50} values were determined using a two-parameter fit (Hill coefficient and IC_{50}) using GraFit software (Erithacus). The $^{app}K_i$* values were calculated from the IC_{50} values using the Cheng-Prusoff relationship for ATP-competitive inhibition.

To determine the selectivity of GSK1904529A, we characterized the inhibition of 45 other kinases using assay conditions developed and optimized individually for each kinase. In addition, GSK1904529A was tested at 0.3 μmol/L in the KinaseProfiler screening (Millipore) against 233 kinases using filter binding activity assays.

Cell culture. Cell lines were obtained from the American Type Culture Collection or the German Collection of Microorganisms and Cell Cultures and routinely cultured in the recommended growth medium. NIH-3T3 cells that overexpress human IGF-IR [NIH-3T3-hIGF-IR (NIH-3T3/LISN)] and IR (NIH-3T3-hIR) were obtained from Dr. Michael Kaleko (Fred Hutchinson Cancer Research Center, Seattle, WA; ref. 14). These cell lines were cultured in DMEM containing 10% fetal bovine serum and 500 μg/mL G418. All cell lines were maintained in humidified incubators at 37°C under 5% CO_2.

IGF-IR and IR phosphorylation assays. NIH-3T3/LISN and NIH-3T3-hIR cell lines were seeded in culture medium in collagen-coated 96-well tissue culture plates (BD Biosciences). After 24 h, cells were treated with DMSO or various concentrations of GSK1904529A and stimulated 2 h later with 30 ng/mL human IGF-I or 3 μg/mL bovine insulin (Sigma-Aldrich) for 15 min. Cells were lysed in radioimmunoprecipitation assay buffer (Roche Diagnostics) and lysates were transferred to wells of 96-well assay plates (MaxiSorp, Nalge Nunc) coated with either anti – IGF-IR (R&D Systems) or anti-IRβ (Santa Cruz Biotechnology). Plates were incubated at 4°C overnight, washed, and incubated with europium-labeled phosphotyrosine antibody PT66 (Perkin-Elmer) for the detection of phosphorylated IGF-IR and IR. Total IGF-IR and IR were detected with anti – IGF-IRβ (Santa Cruz Biotechnology) or anti-IR (Lab Vision/Thermo Fisher Scientific), respectively. Secondary antibodies used were europium-labeled goat anti-rabbit IgG (for IGF-IR) and europium-labeled goat anti-mouse IgG (for IR; Perkin-Elmer). Europium fluorescence was quantified using a Victor Multilabel Counter (excitation, 340 nm/emission, 615 nm; Perkin-Elmer). The ratio of phosphorylated kinase to total kinase was determined, and concentration-response curves were plotted. IC_{50} values were determined from inhibition curves using XLfit4 software (ID Business Solutions).

Cell proliferation assays. Cells were seeded in 96-well dishes, incubated overnight at 37°C, and treated with various concentrations of GSK1904529A for 72 h. For the NIH-3T3/LISN proliferation assays, cells were seeded on collagen-coated 96-well tissue culture plates (BD Biosciences) and allowed to adhere for 24 h. The tissue culture medium was replaced with serum-free medium and the cells were treated with

DMSO or GSK1904529A for 2 h. IGF-I (30 ng/mL) was added and the cells were incubated at 37°C for 72 h. Cell proliferation was quantified using the CellTiter-Glo Luminescent Cell Viability Assay (Promega) following the manufacturer's recommendations. IC_{50} values were determined by using a four-parameter curve fit software package (XLfit4).

Western blotting. Cells were plated in tissue culture dishes and incubated overnight at 37°C. The culture medium was replaced with serum-free medium, and DMSO or GSK1904529A was added to the cells for 4 h before stimulation with IGF-I or insulin for 15 min. Cells were lysed in radioimmunoprecipitation assay buffer and equal amounts of proteins were run on SDS-PAGE gels (Invitrogen). The proteins were then transferred to nitrocellulose membranes and incubated with the antibodies for phospho–IGF-IR/IR ($Tyr^{1135/1136}$), phospho–extracellular signal-regulated kinase (ERK; Thr^{202}/Tyr^{204}), phospho-AKT (Ser^{473}), ERK, and AKT (Cell Signaling Technology) and phospho-IRS-1 (Tyr^{989}), IRS-1, and IGF-IR (Santa Cruz Biotechnology). Antibodies to actin (Sigma-Aldrich) were used to show equal sample loading. Secondary antibodies used were IRDye 700DX–conjugated goat anti-mouse and IRDye 800CW–conjuated goat anti-rabbit (Rockland Immunochemicals). Proteins were detected using the Odyssey Infrared Imager (Li-Cor Biosciences).

Flow cytometry. Cells were seeded into 96-well tissue culture plates overnight at 37°C and treated with DMSO or GSK1904529A for 24 or 48 h. The cells were fixed and stained with propidium iodide to stain nuclei based on the Vindelov method (15). Flow cytometry was done using a FACSCalibur (BD Biosciences) and the fraction of cells in each phase of cell cycle was determined using cell cycle analysis platform in FlowJo software (Tree Star).

In vivo *efficacy studies.* Exponentially growing NIH-3T3/LISN, COLO 205, HT29, and BxPC3 cells were implanted s.c. into the right flank of 8- to 10-wk-old female *nu/nu* CD-1 athymic mice. When the tumors reached 150 to 200 mm^3 in size, mice were block randomized according to tumor size into treatment groups of eight mice each. Mice were treated orally with the vehicle or 30 mg/kg GSK1904529A once or twice daily for 21 d. Mice were weighed and tumors were measured twice weekly using calipers. Tumor volume was calculated using the following formula: (length × $width^2$)/2. The percentage of tumor growth inhibition was calculated on each day of tumor measurement using the following formula: 100 × [1 - (average growth of the drug-treated population/average growth of vehicle-treated control population)].

Metabolic studies. Blood glucose and β-hydroxybutyrate levels were measured using commercial handheld devices: Accucheck (Roche Diagnostics) and MediSense Precision Xtra (Abbott), respectively. Plasma insulin levels were measured by ELISA (Ultra Sensitive Mouse Insulin ELISA kit, Crystal Chem) according to the manufacturers' instructions. For the i.p. glucose tolerance test, food was withdrawn from female *nu/nu* CD-1 mice (three mice per group) for 2 h before administering a single dose of either vehicle or GSK1904529A. Four hours following compound administration, a bolus dose of glucose 2 g/kg was given i.p. Blood glucose measurements were taken before compound administration, before glucose administration, and 15 to 120 min after the glucose challenge.

Pharmacodynamic studies. IGF-IR pharmacodynamic studies were carried out in female *nu/nu* CD-1 mice (three mice per group) bearing NIH-3T3/LISN or COLO 205 tumors of ~500 mm^3, given a single oral dose of either vehicle or GSK1904529A. Four hours after the compound administration, mice were injected via the tail vein with 10 μg of hIGF-I and euthanized after 10 min for collection of tumor tissue and blood. Frozen tumor samples were homogenized in radioimmunoprecipitation assay buffer and 80 μL of each lysate were then added to chilled IGF-IR capture plates that had been prepared as described for the cell-based phosphorylation assays. The plates were then processed using methodology similar to that used for the cell-based IGF-IR phosphorylation assays.

For IR pharmacodynamic studies, a single oral dose of vehicle or GSK1904529A was administered to female *nu/nu* CD-1 mice (three mice per group). Four hours after compound administration, mice were administered 30 units/kg of human insulin i.p. and liver and skeletal muscle (gastrocnemius) were harvested after 2 and 15 min, respectively. Lysate preparation and the detection and quantification of IR phosphorylation were as described above, except that capture plates were prepared for the detection of IR.

Compound concentration analysis. GSK1904529A levels were quantified in blood and whole tissue by protein precipitation in samples with acetonitrile followed by high-performance liquid chromatography/tandem mass spectrometry analysis using positive ion atmospheric pressure chemical ionization or Turbo Ionspray ionization (API 4000 or API 5000, Applied Biosystems). The lower limit of quantification of compound was 10 ng/mL and the assays were linear over a 100- to a 1,000-fold drug concentration range.

Results

Effect of GSK1904529A on IGF-IR and IR kinase activity. GSK1904529A is a potent inhibitor of IGF-IR and the closely related IR with IC_{50} values of 27 ± 10 nmol/L (n = 11) and 25 ± 11 nmol/L (n = 11), respectively, in the *in vitro* kinase

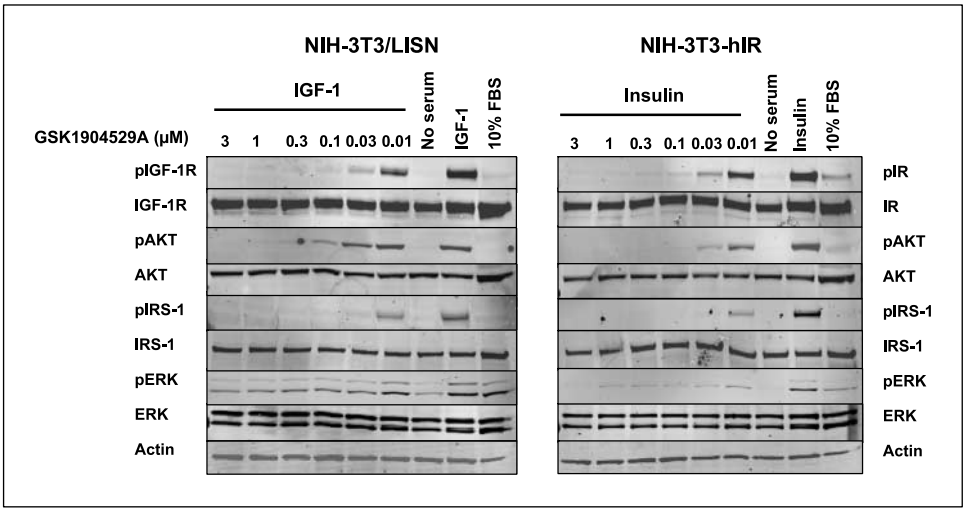

Fig. 1. Effect of GSK1904529A on IGF-I–mediated and IR-mediated signal transduction. NIH-3T3/LISN cells (*left*) and NIH-3T3-hIR cells (*right*) were serum starved and treated with DMSO or GSK1904529A. Four hours later, cells were stimulated with 30 ng/mL IGF-I (*left*) or 3 μg/mL insulin (*right*) for 15 min. Cultures not subject to serum starvation [10% fetal bovine serum (*FBS*)] and cells left unstimulated (*No serum*) were used as controls. Cell lysates were resolved by SDS-PAGE and analyzed by Western blotting. Antibodies to actin were used to show equal sample loading.

Table 1. Activity of GSK1904529A in cell proliferation assays

Cell line	Tumor	IC_{50} (nmol/L)*
NCI-H929	Multiple myeloma	81 ± 42
MOLP-8		96 ± 18
LP-1		104 ± 32
KMS-12-BM		113 ± 27
L-363		165 ± 94
EJM		>30,000
HUNS-1		>30,000
JJN-3		>30,000
TC-71	Ewing's sarcoma	35 ± 16
SK-ES		61 ± 12
RD-ES		62 ± 20
A673		>30,000
MHH-ES-1		>30,000
SK-N-MC	Askin's tumor	43 ± 15
COLO 205	Colon	124 ± 52
HT29		104 ± 67
MCF7	Breast	137 ± 7
MX1		189 ± 89
MDA-MB-468		>20,000
KARPAS-299	Anaplastic large cell lymphoma	>30,000
L-82		>30,000
SR-786		>30,000
SU-DHL-1		>30,000
SUP-M2		>30,000
A549	Lung	>20,000
NCI-H1299		>20,000
HELA	Cervix	>20,000
HN5	Head and neck	>20,000
LNCAP	Prostate	>20,000
SKOV3	Ovary	>20,000
PREC	Normal prostate epithelium	68 ± 25 †
HMEC	Normal mammary epithelium	>20,000
HFF	Normal foreskin fibroblast	>20,000
HUVEC	Normal umbilical vein epithelium	>20,000
LISN+IGF1	Murine fibroblast overexpressing full-length human IGF-IR	60 ± 20

*Mean ± SD.
† Anomalous inhibition curves with maximum inhibition of 45% to 68%.

assays with purified enzymes. The compound is a reversible, ATP-competitive inhibitor. Owing to time-dependent inhibition of GSK1904529A, indicated by the curvilinear nature of the reaction progress curve and its slow off-rate (data not shown), equilibrium between enzyme-inhibitor binding is established slowly. Therefore, apparent K_i values were estimated after a 6-hour incubation and 2-hour reaction time. K_i values were 1.6 ± 0.1 nmol/L (n = 2) and 1.3 ± 0.1 nmol/L (n = 3) against IGF-IR and IR, respectively. The low apparent K_i values obtained, relative to the IC_{50}s, are a result of the time-dependent binding of the compound and the shorter incubation and reaction times used in determination of the IC_{50}s. To evaluate the selectivity of GSK1904529A, it was tested against 45 other serine/threonine and tyrosine kinases and showed poor activity in all kinases (IC_{50} > 1 μmol/L; Supplementary Table S1). Inhibition of ligand-dependent IGF-IR and IR autophosphorylation in intact cells by GSK1904529A was assessed in the NIH-3T3/LISN and NIH-3T3-hIR cells, respectively. GSK1904529A potently inhibited phosphorylation of IGF-IR (IC_{50} = 22 ± 8 nmol/L) and IR (IC_{50} = 19 ± 8 nmol/L), consistent with the activity against the purified enzymes.

Effect of GSK1904529A on signaling pathways. We next investigated the effects of GSK1904529A on the signal transduction pathways mediated by IGF-IR and IR. Whole-cell extracts of unstimulated and ligand-stimulated cells were analyzed by Western blotting. Low basal levels of IGF-IR/IR phosphorylation were observed in the absence of serum (Fig. 1). On ligand stimulation, a large increase in phosphorylated IGF-IR and IR was observed, indicative of receptor activation. Phosphorylation of the downstream signaling kinases, including AKT, IRS-1, and ERK, in response to ligand stimulation was also observed. GSK1904529A profoundly inhibited the ligand-induced phosphorylation of IGF-IR and IR at concentrations >0.01 μmol/L. In parallel, decreases in phosphorylated AKT, IRS-1, and ERK were also observed, indicating that inhibition of the receptor kinase phosphorylation by GSK1904529A was sufficient to block the major downstream signaling pathways. To study the effects of GSK1904529A in an unmodified tumor cell line of epithelial origin, similar experiments were carried out in MCF-7 cells. Almost identical results were obtained when the cells were stimulated with either IGF-I or insulin (Supplementary Fig. S2).

Effect of GSK1904529A on tumor cell proliferation. GSK1904529A was then tested in a panel of cell lines derived from a variety of solid and hematologic tumors (Table 1). NIH-3T3/LISN cells, whose growth is dependent on IGF-I (14), were used as a control cell line and are highly sensitive to growth inhibition by GSK1904529A (IC_{50} = 60 nmol/L). IC_{50}s for

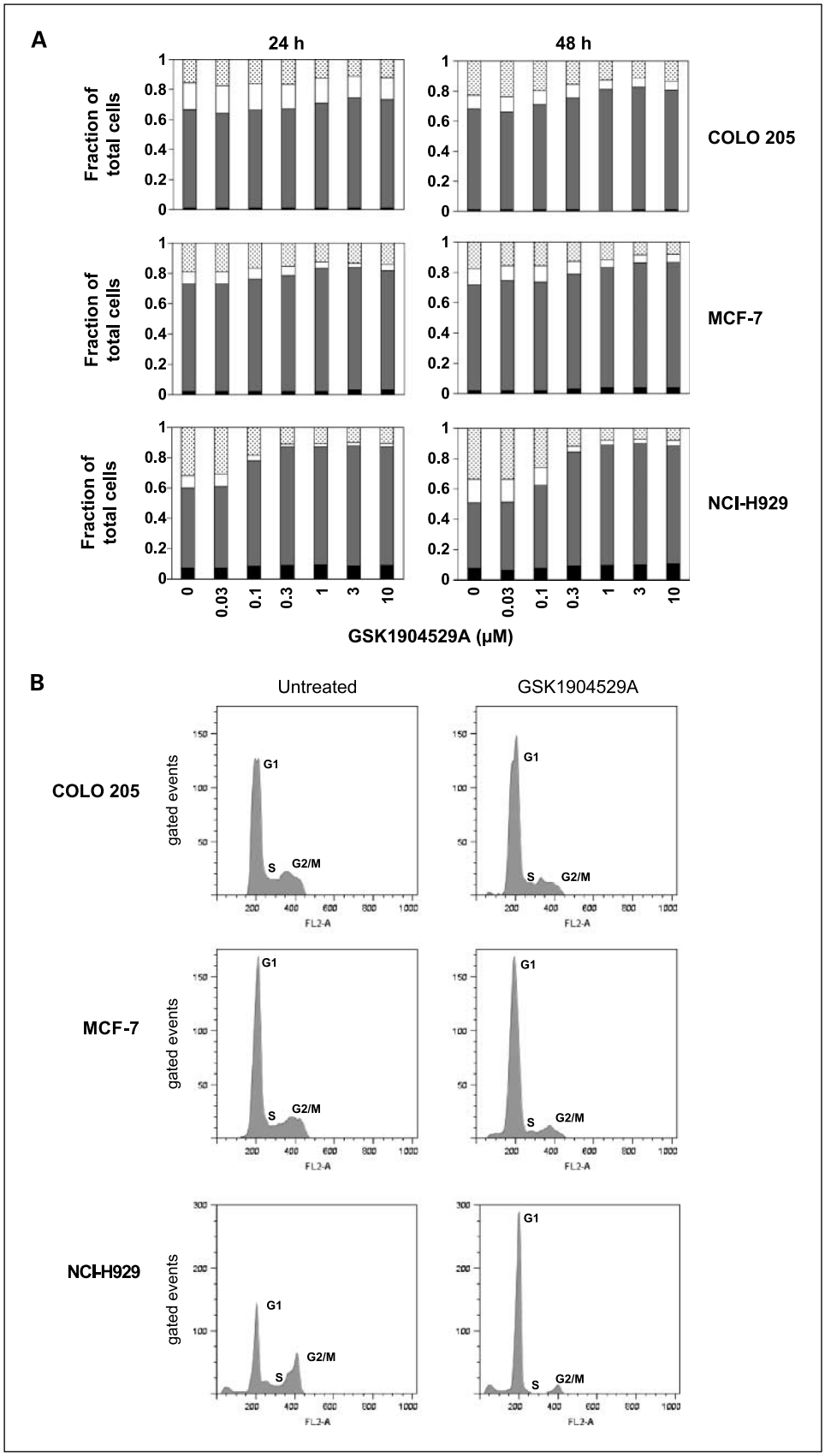

Fig. 2. Cell cycle effects of GSK1904529A. COLO 205, MCF-7, and NCI-H929 cells were treated with DMSO or GSK1904529A for 24 or 48 h. Nuclei were fixed, stained with propidium iodide, and analyzed by flow cytometry. *A,* the fraction of cells in sub-G_1 (*black*) G_1 (2N; *gray*), S (*white*), and G_2-M (4N; *speckled*) are shown. The experiment was repeated twice; a representative experiment is shown. *B,* representative histograms from cells treated with 1 μmol/L GSK1904529A for 48 h. Cell cycle phases are indicated.

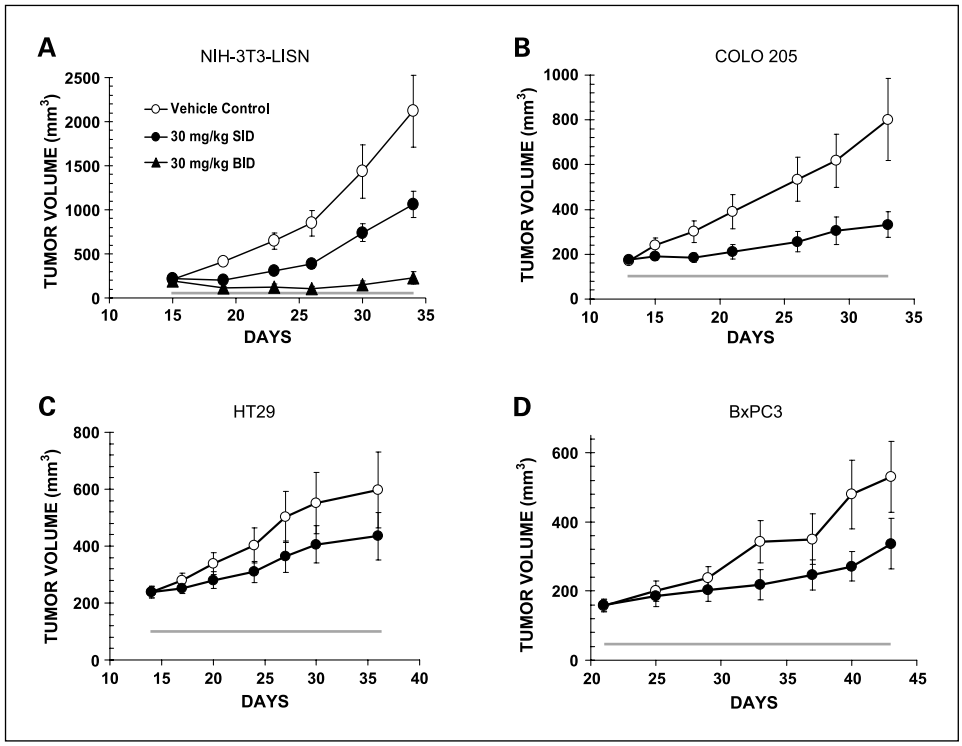

Fig. 3. Antitumor activity of GSK1904529A *in vivo*. Female nude mice bearing tumor xenografts of NIH-3T3/LISN (*A*), COLO 205 (*B*), HT29 (*C*), or BxPC3 (*D*) were treated with vehicle (○) and 30 mg/kg GSK1904529A once daily (*SID*; ●) or twice daily (*BID*; ▲) for 21 d. Duration of treatment is shown by the horizontal gray line at the bottom of the graphs. Tumors were measured twice per week. Points, mean tumor volumes; bars, SE.

GSK1904529A in other tumor cell lines ranged from 35 nmol/L to >30 μmol/L (Table 1). The tumor histologic types showing the greatest sensitivity to this compound were Ewing's sarcoma and multiple myeloma, where IC_{50}s in three of five Ewing's sarcoma cell lines were <100 nmol/L and IC_{50}s in five of eight multiple myeloma cell lines were <200 nmol/L. SK-N-MC, a cell line derived from an Askin's tumor, which belongs to the Ewing's sarcoma family of tumors, is also sensitive to GSK1904529A, having an IC_{50} of 43 nmol/L. Both colon carcinoma lines tested and two of three breast cancer cell lines were sensitive to GSK1904529A (IC_{50} = 100-200 nmol/L). All of the other cell lines, with the exception of PREC (normal prostate epithelial cells), were insensitive to the compound (Table 1).

Cell cycle profiles of cell lines treated with GSK1904529A. We next examined the cell cycle distribution of cells treated with GSK1904529A. COLO 205, MCF-7, and NCI-H929 cells, which are highly sensitive to GSK1904529A (Table 1), were selected for this analysis. Exponentially growing cells were treated with increasing concentrations of GSK1904529A for 24 and 48 hours and analyzed by flow cytometry (Fig. 2). GSK1904529A-treated cells showed increased accumulation in G_1 and decreased accumulation in S and G_2-M phases of the cell cycle. The effects were most pronounced in the NCI-H929 multiple myeloma cells. After 48 hours of compound treatment (1 μmol/L), the percentage of cells in the G_1 phase increased from 65% to 78% in COLO 205, 67% to 76% in MCF-7, and 42% to 79% in NCI-H929 cells. Conversely, the percentage of cells in S phase decreased from 9% to 6% in COLO 205, 10% to 5% in MCF-7, and 15% to 3% in NCI-H929 cells. The percentage of cells in the G_2 phase also decreased from 22% to 12% in COLO 205, 17% to 11% in MCF-7, and 33% to 8% in NCI-H929 cells (Fig. 2). There were no significant changes in the number of cells showing a sub-2N DNA content up to 72 hours (Fig. 2; data not shown). These results suggest that the primary effect of GSK1904529A is to arrest cells at the G_1 phase of the cell cycle.

In vivo *activity of GSK1904529A.* The ability of GSK1904529A to affect tumor growth *in vivo* was first assessed in xenografts of NIH-3T3/LISN and COLO 205 cells. Treatment of NIH-3T3/LISN tumor-bearing animals at 30 mg/kg, orally, once daily resulted in a 56% inhibition of tumor growth compared with vehicle-treated control animals (calculated at the end of the treatment period; Fig. 3A). Twice-daily administration at 30 mg/kg resulted in 98% inhibition of tumor growth. There was no significant decrease in body weight of mice treated with vehicle or 30 mg/kg GSK1904529A on the once-daily schedule (Supplementary Fig. S3A). Body weight loss of 13% was seen after 5 days of treatment in the 30 mg/kg, twice-daily group. This weight loss remained steady at 11% to 13% and recovered to near baseline (within 2% of baseline) 6 days after the cessation of treatment (Supplementary Fig. S3A; data not shown). In animals bearing COLO 205 xenografts, maximal tumor growth inhibition of 75% was shown with 30 mg/kg, once-daily treatment with a body weight loss of between 5% and 10% throughout the treatment duration (Fig. 3B; Supplementary Fig. S3B). However, the 30 mg/kg, twice-daily dose group showed >20% body weight loss and daily compound administration had to be suspended (data not shown).

GSK1904529 was also tested in HT29 and BxPC3 xenografts at a well-tolerated dose of 30 mg/kg, once daily. Tumor growth inhibition of 47% and 52%, respectively, was observed at the end of the treatment period relative to vehicle controls (Fig. 3C and D), with no significant changes in body weight (Supplementary Fig. S3C and D).

Modulation of IGF-IR activity **in vivo.** To determine the effect of GSK1904529A on the activity of the target *in vivo* and to develop preliminary pharmacokinetic-pharmacodynamic relationships, we assessed the phosphorylation of IGF-IR in tumor xenografts. Low levels of phosphorylated IGF-IR were present in the tumors of control mice (Fig. 4A, *V+S*). Animals injected with hIGF-I (*V+IGF-I*) showed a 14-fold increase of phosphorylated IGF-IR levels in the tumors. A single oral dose of GSK1904529A given at 1, 3, 10, and 30 mg/kg resulted in 57%, 75%, 95%, and 99% decrease in IGF-I–induced IGF-IR phosphorylation, respectively. Analysis of the blood and tumor compound concentrations showed a dose-dependent increase in compound, with blood having ~2-fold higher concentrations than tumor tissue at all but the highest concentration. Complete inhibition of IGF-IR phosphorylation was achieved with GSK1904529A blood levels of ~3,000 ng/mL (3.5 μmol/L). A similar dose-dependent decrease in phospho–IGF-IR by GSK1904529A was observed in xenografts of COLO 205, a cell line that has physiologically relevant levels of the IGF-IR receptor (Supplementary Fig. S4).

In a time course study (Fig. 4B), a single 30 mg/kg dose of GSK1904529A reduced ligand-induced IGF-IR phosphorylation in NIH-3T3-LISN tumor xenografts by >90% 4 to 8 hours after compound administration. A 76% reduction in phosphorylated IGF-IR was observed at 24 hours, with no significant reduction at 48 and 72 hours. GSK1904529A levels in the tumor and blood were similar and remained high between 1 and 8 hours, decreased at 24 and 48 hours, and were undetectable by 72 hours. Consistent with the dose-response study, >90% inhibition of IGF-IR phosphorylation was achieved with GSK1904529A blood levels of ~2,500 ng/mL (3 μmol/L). Interestingly, although the blood and tumor levels of the compound were similar at the 1- and 24-hour time points, no inhibition of phosphorylated IGF-IR was observed at the 1-hour point. This may be due to the time-dependent binding of GSK1904529A to the receptor.

Effect of IGF-IR/IR inhibition on blood glucose levels. The *in vitro* assays indicated that GSK1904529A inhibited activity of IR. Because glucose homeostasis *in vivo* is maintained through the insulin-mediated uptake of glucose in skeletal muscle and suppression of glucose production in the liver (16), the effect of GSK1904529A on phosphorylation of IR in these tissues was determined (Fig. 5). Low levels of IR phosphorylation were observed in control mice (*V+S*), with an increase in IR phosphorylation following insulin administration (*V+Ins*). A dose-dependent decrease in phosphorylated IR was seen in both liver (Fig. 5A) and muscle (Fig. 5B), with substantial reduction occurring at doses ≥30 mg/kg. GSK1904529A concentration in blood and tissue shows a dose-dependent increase with a plateau at the highest doses tested. Signaling downstream of the IR was examined in the liver tissue of mice treated with GSK1904529A (Fig. 5C). A dose-dependent decrease in IR phosphorylation was detected. Although substantial inhibition of ligand-dependent IR phosphorylation was evident at 30 mg/kg, a more modest decrease in the phosphorylation of IRS and AKT was observed, suggesting that inhibition of IR signaling in the liver, downstream of the receptor, requires a higher dose of GSK1904529A than that required to inhibit IGF-IR–dependent tumor growth. GSK1904529A had no effect on basal levels of IR phosphorylation or basal IR signaling (Fig. 5C).

To assess the biological effect of IR inhibition, blood glucose measurements were done on mice treated with GSK1904529A at 30 mg/kg for 21 days (Supplementary Fig. S5A). There were no significant alterations in the blood glucose levels in mice treated once or twice daily with GSK1904529A when compared with vehicle-treated mice. No changes in β-hydroxybutyrate levels, which are used to monitor ketosis that occurs as a result of an inability of cells to obtain glucose, were observed (Supplementary Fig. S5B). Blood insulin levels were also monitored along with glucose in mice after a single dose of GSK1904529A (Fig. 5D). No changes in blood glucose levels were observed, consistent with the results obtained with chronic administration. However, insulin levels increased from 0.7 to 33 ng/mL within 6 hours and returned to near-normal levels in 24 hours, suggesting that increased insulin production may contribute to maintaining glucose homeostasis by compensating for a deficiency in intracellular insulin signaling.

To further examine the effect of GSK1904529A on glucose homeostasis, a glucose tolerance test was done (Supplementary

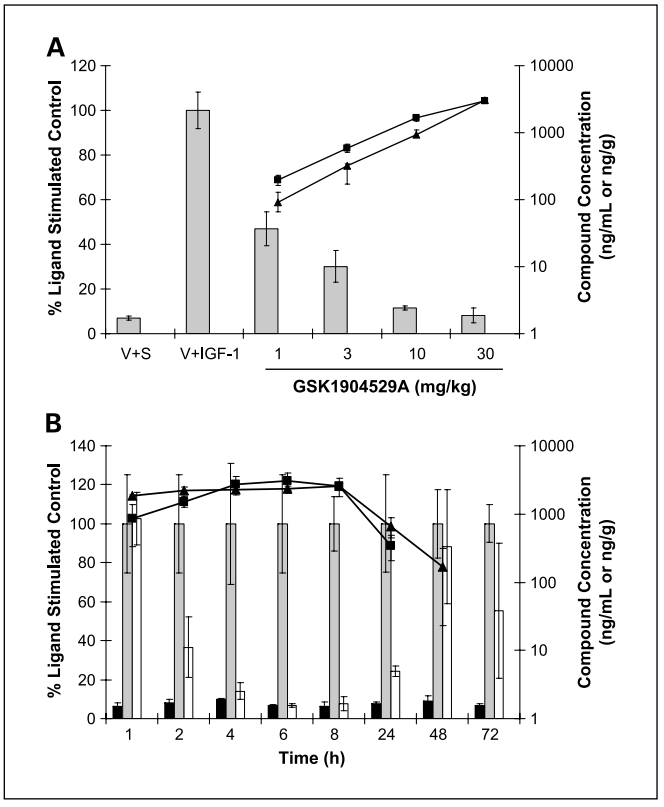

Fig. 4. Effect of GSK1904529A on IGF-IR phosphorylation *in vivo. A,* female nude mice bearing NIH-3T3/LISN tumors (three mice per group) were treated with vehicle (*V*) or GSK1904529A for 4 h followed by injection of IGF-I i.v. Control animals were injected with saline (*V+S*). After 10 min, blood and tumor tissue were collected. Lysates were prepared from half the tumor samples and analyzed for levels of phospho – IGF-IR and total IGF-IR. The ratios of phospho – IGF-IR to IGF-IR were calculated and expressed as a percentage of the ratio obtained in ligand-stimulated controls. Columns and points, mean; bars, SD. The concentration of GSK1904529A in the tumor (*triangles*; ng/g) and blood (*squares*; ng/mL) was quantified. For the time course study (*B*), tumor-bearing animals (three mice per group) were treated with vehicle (*black columns*) or 30 mg/kg GSK1904529A and administered with IGF-I 10 min before collection of blood and tumor tissue at each time point. Gray columns, IGF-I stimulation; white columns, IGF-I stimulation with GSK1904529A treatment. The concentration of GSK1904529A in the tumor (*triangles*) and blood (*squares*) was also quantified. Missing points indicate that compound concentration was below detection limits.

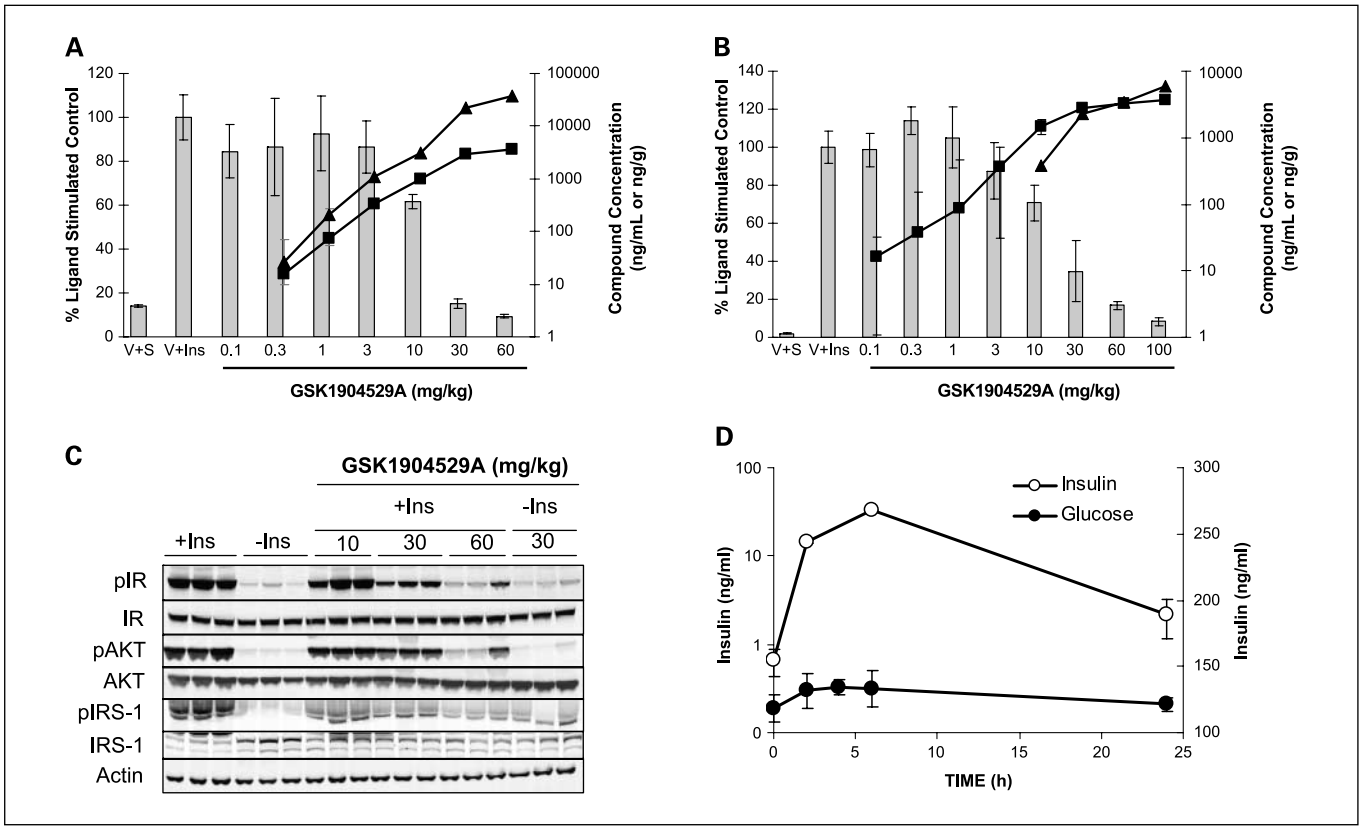

Fig. 5. Effect of GSK1904529A on IR phosphorylation and glucose metabolism. IR phosphorylation studies were carried out in naive nude mice (three mice per group) treated with vehicle or GSK1904529A followed 4 h later with human insulin i.p. Control animals were administered vehicle and later injected with saline (*V+S*). Liver tissue was collected after 2 min (*A*), and skeletal muscle was collected after 15 min (*B*) to measure IR phosphorylation. The ratio of phospho-IR (*pIR*) to IR expressed as a percentage of the ratio in the ligand-stimulated control samples is shown. Columns and points, mean; bars, SD. The concentration of GSK1904529A in blood (*squares*; ng/mL) and tissue (*triangles*; ng/g) was also determined. Missing points indicate that compound concentration was below detection limits. *C,* Western blotting was carried out on liver tissue lysates from naive *nu/nu* CD-1 mice treated with vehicle or a single dose of GSK1904529A (10-60 mg/kg, three mice per group) followed 4 h later with human insulin i.p. (*+Ins*) or saline (*-Ins*). Antibodies to actin were used to show equal sample loading. *D,* blood glucose was measured in naive *nu/nu* CD-1 mice (three mice per group) treated with a single dose of 30 mg/kg GSK1904529A. Measurements were made before compound administration (time 0) and at 2, 4, 6, and 24 h after compound administration. ○, insulin; ●, glucose. No data were collected at the 2-h time point for insulin measurement.

Fig. S5C). Mice treated with the vehicle showed an increase in blood glucose levels 15 minutes following glucose administration, which returned to baseline by 60 minutes. In mice pretreated with 30 mg/kg GSK1904529A, there was an increase in the peak blood glucose level over the vehicle-treated mice at 15 minutes following glucose administration (285 mg/dL compared with 214 mg/dL). However, these levels returned to normal by 60 minutes.

Discussion

GSK1904529A is the lead compound from a class of imidazopyridines that was selected for detailed characterization based on its high degree of selectivity for IGF-IR and IR. The compound was first tested in a panel of 47 kinases and was found to have potent activity only against IGF-IR and IR. To obtain additional selectivity information, GSK1904529A was tested in 233 unique protein kinase assays available though the KinaseProfiler panel (Supplementary Table S2). At a concentration of 0.3 μmol/L, only three other kinases tested (PTK5, FER, and FLT4) were inhibited >50% by GSK1904529A. At a concentration of 3 μmol/L, 20 kinases were inhibited >50%, but only 11 of 19 of these, for which IC_{50} values were determined, gave values <1 μmol/L (Supplementary Table S2). The discrepancy in IC_{50} values for Aurora A between data generated at GlaxoSmithKline (Supplementary Table S1) and the KinaseProfiler screen (Supplementary Table S2) is likely due to the presence of the Aurora A accessory protein TPX2 in the GlaxoSmithKline assays.[3] Overall, these data suggest that GSK1904529A is a highly selective IGF-IR and IR inhibitor.

The primary cell cycle effect of GSK1904529A in the cancer cell lines tested was accumulation in G_1 phase. IGF-IR drives progression through the cell cycle by activating the PI3K/AKT and MAPK pathways, leading to transcriptional up-regulation of the G_1-phase regulators cyclin D1, cyclin-dependent kinase 4, and cyclin E (1). GSK1904529A blocks IGF-IR–mediated activation of the PI3K/AKT and MAPK signaling pathways in cells. In addition to accumulation of cells in G_1, inhibition of IGF-IR has been shown to induce apoptosis in cultured tumor cells (17–19). Moreover, IGF-IR has been shown to inhibit anoikis (20), and apoptosis induced by UV radiation (21), chemotherapeutic drugs (22), and the oncogene c-myc (23). It will be interesting to examine the activity of GSK1904529A as a facilitator of apoptosis under these conditions.

[3] Unpublished observations, E.R. Wood, GlaxoSmithKline, Research Triangle Park, North Carolina.

Several multiple myeloma and Ewing's sarcoma cell lines were sensitive to GSK1904529A *in vitro*. IGF-IR has been shown to play an important role in the growth and survival of human tumor cell lines originating from multiple myeloma and Ewing's sarcoma (17, 24–27). Clinically, treatment of multiple myeloma patients with an IGF-IR monoclonal antibody in combination with dexamethasone leads to partial and complete responses (28). Despite the general sensitivity of multiple myeloma cell lines, the EJM, HUNS-1, and JJN-3 cell lines were relatively resistant to GSK1904529A-induced growth inhibition (IC_{50}s > 30 μmol/L). The protein tyrosine phosphatase CD45 negatively regulates IGF-IR signaling in multiple myeloma cells and that the growth of $CD45^+$ multiple myeloma cells is refractory to anti–IGF-IR monoclonal antibodies (29, 30). RNA expression data suggest that the HUNS-1 cell line has high level of CD45 mRNA levels compared with sensitive cell lines MOLP-8, LP-1, and KMS-12BM, which may explain the lack of sensitivity of HUNS-1 cells to GSK1904529A (data not shown). However, another resistant cell line, EJM, had very similar (low) CD45 mRNA levels compared with the sensitive cell lines, suggesting that CD45 expression alone is not the cause of resistance to these cells.

Activation of the IGF-IR signaling pathway is involved in the growth, invasion, and metastasis of Ewing's sarcoma (31). More than 85% of Ewing's family tumors harbor a translocation between the *EWS* gene and the FLI1 transcription factor, and silencing the expression of this transcription factor increases the susceptibility of Ewing's sarcoma cells to apoptosis (32–34). EWS-FLI1 has been shown to transcriptionally repress the expression of IGFBP-3, the main circulating carrier protein for IGFs (34). IGFBP-3 inhibits IGF-IR–mediated signaling by preventing the interaction of IGFs with IGF-IR. Thus, transcriptional repression of IGFBP-3 by EWS-FLI1 could reactivate the IGF-IR signaling pathway and thereby confer dependency on IGF-IR for cell growth. Although we have confirmed that EWS-FLI1 is expressed in each of the Ewing's sarcoma cell lines used in our study (data not shown), we have not confirmed a role for EWS-FLI1–mediated transcriptional repression of IGFBP-3 in the growth of these lines. IGF-IR–independent signaling pathways may also play a role in the growth of Ewing's sarcoma cells, as not all Ewing's sarcoma cell lines used in our study were sensitive to growth inhibition by GSK1904529A. EWS-FLI1 has been shown to transactivate the expression of several genes besides those regulated by the IGF-IR pathway, which could contribute to the aberrant growth of Ewing's sarcoma cells (35).

GSK1904529A inhibited IGF-IR and IR kinase activities with similar potencies and compromised IR activation in cells and *in vivo*. This is consistent with the fact that these two highly related kinases share 85% sequence homology in the kinase binding domains and have identical ATP binding clefts (36). In addition to its role in glucose metabolism, recent evidence suggests a role for IR signaling in cancer. IR-A is an isoform of IR, generated by alternative splicing, which is typically expressed in fetal tissues but is also expressed in thyroid, ovarian, breast, and colon cancers and leiomyosarcomas (37–40). IR-A stimulates DNA synthesis by binding with high affinity to IGF-II, thus serving as a second physiologic receptor for this ligand (41). IR-A has also been shown to heterodimerize with IGF-IR and these hybrid receptors can stimulate cell motility in response to IGF-II, IGF-I, and insulin (42, 43). IR-A may therefore function as a tumor promoter under certain conditions, and inhibition of IR-A kinase activity is predicted to antagonize this oncogenic potential. More recently, IGF-I was shown to activate both splice variants of IR, resulting in activation of IRS-2 and PI3K pathway leading to increased cell viability and protection from apoptosis (44). Thus, the anticancer properties of ATP-competitive IGF-IR inhibitors such as GSK1904529A may be mediated in part through inhibition of IR-A. Moreover, this ability to inhibit both IGF-IR and IR kinase activity potentially provides a therapeutic advantage over anti–IGF-IR monoclonal antibodies.

Because GSK1904529A inhibits the activity of the IR in muscle and liver tissues *in vivo* at blood concentrations comparable with those required for antitumor activity, the lack of a hyperglycemic response is surprising. However, our *in vivo* data show that inhibition of downstream IR signaling in the liver requires a higher dose of GSK1904529A than that required to inhibit IGF-IR–dependent tumor growth and suggest that few active IR molecules are needed for maintaining IR signaling. Lack of hyperglycemia may also be explained by the increase in circulating insulin level or a potential intracellular feedback mechanism of IRS-1 and AKT activation, similar to those observed with mammalian target of rapamycin and AKT inhibitors (45, 46). Furthermore, no evidence of hyperglycemia was observed in preclinical studies on another IGF-IR kinase inhibitor, NVP-AE541 (47). The lack of a hyperglycemic response by GSK1904529A at efficacious doses in preclinical studies has positive implications in the clinic because hyperglycemia has been observed in clinical trials on IGF-IR antibodies (9). However, we observed that daily dosing of GSK1904529A at a dose that was not well tolerated (100 mg/kg, once daily) induced sustained increases in glucose and insulin levels in both tumor-bearing and naive athymic mice (data not shown). These data underscore the potential for GSK1904529A to induce a hyperglycemic response in patients but suggest that the doses required for this response may be higher than what is needed for antitumor efficacy.

In conclusion, we have shown that GSK1904529A is a potent and selective modulator of IGF-IR activity *in vitro*, with robust antitumor activity in tumor xenograft models. Preclinical data for GSK1904529A and other IGF-IR inhibitors provide a rationale for using IGF-IR inhibitors in patients with multiple myeloma, sarcomas, and tumors of the breast, prostate, and colon (17, 47). Loss of imprinting of the *IGF-II* gene has been implicated in the etiology of Wilms' tumor (48). In addition, compelling evidence indicates a role for IGF-IR signaling in gastrointestinal stromal tumors (49) and in chronic myelogenous leukemia (50), extending the potential clinical opportunities for GSK1904529A as an anticancer therapeutic agent. Recent encouraging results with an IGF-IR antibody in lung cancers (11), and ongoing clinical trials in other cancers (8), may expand the range of susceptible tumors. Simple overexpression of the receptor is unlikely to predict responsiveness of tumors to these inhibitors, and methods to identify the activation state of the pathway measured by phosphorylated IGF-IR or IGF-I expression may be useful (1). Beyond this, identification of molecular signatures of responsiveness, derived from transcriptional profiling or proteome analysis, may help identify patients who will benefit from IGF-IR–targeted therapies.

Disclosure of Potential Conflicts of Interest

All authors are current or former employees of GlaxoSmithKline.

References

1. Pollak MN, Schernhammer ES, Hankinson SE. Insulin-like growth factors and neoplasia. Nature Rev Cancer 2004;4:505–18.
2. Hartog H, Wesseling J, Marike BH, van der Graaf WTA. The insulin-like growth factor 1 receptor in cancer: old focus, new future. Eur J Cancer 2007;43:1895–904.
3. Sell C, Rubini M, Rubin R, Liu J-P, Efstratiadis A, Baserga R. Simian virus 40 large tumor antigen is unable to transform mouse embryo fibroblasts lacking type 1 insulin-like growth factor receptor. Proc Natl Acad Sci U S A 1993;90:11217–21.
4. Resnicoff M, Coppola D, Sell C, Rubin R, Ferrone S, Baserga R. Growth inhibition of human melanoma cells in nude mice by antisense strategies to the type 1 insulin-like growth factor receptor. Cancer Res 1994;54:4848–50.
5. Hoffmann F, Garcia-Echeverria C. Blocking insulin-like growth factor-1 receptor as a strategy for targeting cancer. Drug Disc Today 2005;10:1041–7.
6. Yakar S, LeRoith D, Brodt P. The role of the growth hormone/insulin-like growth factor axis in tumor growth and progression: lessons from animal models. Cytokine Growth Factor Rev 2005;16:407–20.
7. Baserga R, Peruzzi F, Reiss K. The IGF-1 receptor in cancer biology. Int J Cancer 2003;107:873–7.
8. Paz K, Hadari YR. Targeted therapy of the insulin-like growth factor-1 receptor in cancer. Combinatorial Chem High Throughput Screening 2008;11:62–9.
9. Sachdev D. Drug evaluation: CP-751871, a human antibody against type I insulin-like growth factor receptor for the potential treatment of cancer. Curr Opinion Mol Ther 2007;9:299–304.
10. Olmos D, Okuno S, Schuetze SM, et al. Safety, pharmacokinetics and preliminary activity of the anti-IGF-1R antibody CP-751,871 in patients with sarcoma. J Clin Oncol 2008;26:10501.
11. Karp DD, Paz-Ares LG, Novello S, et al. High activity of the anti-IGF-1R antibody CP-751,871 in combination with paclitaxel and carboplatin in squamous NSCLC. J Clin Oncol 2008;26:8015.
12. Nahta R, Yu D, Hung M-C, Hortobyagi GN, Esteva FJ. Mechanisms of disease: understanding resistance to HER2-targeted therapy in human breast cancer. Nat Clin Prac 2006;3:269–80.
13. Milano A, Dal Lago L, Sotiriou C, Piccart M, Cardoso F. What clinicians need to know about antiestrogen resistance in breast cancer. Eur J Cancer 2006;42:2692–705.
14. Kaleko M, Rutter W, Miller D. Overexpression of the human insulinlike growth factor I receptor promotes ligand-dependent neoplastic transformation. Mol Cell Biol 1990;10:464–73.
15. Vindelov LI, Christensen IJ, Jensen J, Nissen NI. Limits of detection of nuclear DNA abnormalities by flow cytometric DNA analysis: results obtained by a set of methods for sample-storage, staining and international standardization. Cytometry 1983;3:332–8.
16. Kim J, Wei Y, Sowers JR. Role of mitochondrial dysfunction in insulin resistance. Circ Res 2008;102:401–14.
17. Mitsiades CS, Mitsiades NS, McMullan CJ, et al. Inhibition of the insulin-like growth factor receptor-1 tyrosine kinase activity as a therapeutic strategy for multiple myeloma, other hematological malignancies, and solid tumors. Cancer Cell 2004;5:221–30.
18. Haluska P, Carboni JM, Loegering DA, et al. *In vitro* and *in vivo* antitumor effects of the dual insulin-like growth factor-1/insulin receptor inhibitor, BMS-554417. Cancer Res 2006;66:362–71.
19. Girnita A, Girnita L, del Prete F, Bartolazzi A, Larsson O, Axelson M. Cyclolignans as inhibitors of the insulin-like growth factor-1 receptor and malignant cell growth. Cancer Res 2004;64:236–42.
20. Chattopadhyay A, Carpenter G. PLC-γ1 is required for IGF-1 protection from cell death induced by loss of extracellular matrix adhesion. J Cell Sci 2002;115:2233–9.
21. Kuhn C, Hurwitz SA, Kumar MG, Cotton J, Spandau DF. Activation of the insulin-like growth factor-1 receptor promotes the survival of human keratinocytes following ultraviolet B irradiation. Int J Cancer 1999;80:431–8.
22. Lee Y-J, Imsumran A, park M-Y, et al. Adenovirus expressing shRNA to IGF-1R enhances the chemosensitivity of lung cancer cell lines by blocking IGF-1 pathway. Lung Cancer 2007;55:279–86.
23. Harrington EA, Bennett MR, Fanidi A, Evan GI. c-Myc-induced apoptosis in fibroblasts is inhibited by specific cytokines. EMBO J 1994;13:3286–95.
24. Georgii-Hemming P, Wiklund HJ, Ljunggren O, Nilsson K. Insulin-like growth factor 1 is a growth and survival factor in human multiple myeloma cell lines. Blood 1996;88:2250–8.
25. Benini S, Manara MC, Baldini N, et al. Inhibition of insulin-like growth factor 1 receptor increases the antitumor activity of doxorubicin and vincristine against Ewing's sarcoma cells. Clin Cancer Res 2001;7:1790–7.
26. Manara MC, Landuzzi L, Nanni P, et al. Preclinical *in vivo* study of new insulin-like growth factor 1 receptor-specific inhibitor in Ewing's sarcoma. Clin Cancer Res 2007;13:11322–30.
27. Scotlandi K, Manara MC, Nicoletti G, et al. Antitumor activity of the insulin-like growth factor 1 receptor kinase inhibitor NVP-AEW541 in musculoskeletal tumors. Cancer Res 2005;65:3868–76.
28. Lacy MQ, Alsina M, Fonseca R, et al. Phase I, pharmacokinetic and pharmacodynamic study of the anti-insulinlike growth factor type 1 receptor monoclonal antibody CP-751,871 in patients with multiple myeloma. J Clin Oncol 2008;26:3196–203.
29. Deschamps G, Pellat-Deceunynck C, Szpak Y, Bataille R, Robillard N, Amiot M. The magnitude of Akt/phosphatidylinositol 3′ kinase proliferating signaling is related to CD45 expression in human myeloma cells. J Immunol 2004;173:4953–9.
30. Deschamps G, Wuilleme-Toumi S, Trichet V, et al. CD45neg but not CD45pos human myeloma cells are sensitive to the inhibition of IGF-1signaling by a murine anti-IGF-1R monoclonal antibody, mAVE1642. J Immunol 2006;177:4953–9.
31. Leavey PJ, Collier AB. Ewing sarcoma: prognostic criteria, outcomes and future treatment. Expert Rev Anticancer Ther 2008;8:617–24.
32. Arvand A, Denny CT. Biology of EWS/ETS fusions in Ewing's family tumors. Oncogene 2001;20:5747–54.
33. Yi H-K, Fujimura Y, Ouchida M, Prasad DDK, Rao VN, Reddy ESP. Inhibition of apoptosis by normal and aberrant Fli-1 and erg proteins involved in human solid tumors and leukemias. Oncogene 1997;14:1259–68.
34. Prieur A, Tirode F, Cohen P, Delattre O. EWS/FLI-1 silencing and gene profiling of Ewing cells reveal downstream oncogenic pathways and a crucial role for repression of insulin-like growth factor binding protein 3. Mol Cell Biol 2004;24:7275–83.
35. Smith R, Owen LA, Trem DJ, et al. Expression profiling of EWS/FLI identifies NKX2.2 as a critical target gene in Ewing's sarcoma. Cancer Cell 2006;9:405–16.
36. Favelyukis S, Till JH, Hubbard SR, Miller WT. Structure and autoregulation of the insulin-like growth factor-1 receptor kinase. Nature Struc Biol 2001;8:1058–63.
37. Kalli K, Falowo OI, Bale LK, Zschunke MA, Roche PC, Conover CA. Functional insulin receptors on human epithelial ovarian carcinoma cells: implications for IGF-2 mitogenic signaling. Endocrinol 2002;143:3259–67.
38. Vella V, Pandini G, Sciacca L, et al. A novel autocrine loop involving IGF-2 and the insulin receptor isoform-A stimulates growth of thyroid cancer. J Clin Endocrinol Metab 2003;143:3259–67.
39. Sciacca L, Costantino A, Pandini G, et al. Insulin receptor activation by IGF-2 in breast cancers: evidence for a new autocrine/paracrine mechanism. Oncogene 1999;18:2471–9.
40. Sciacca L, Mineo R, Pandini G, Murabito A, Vigneri R, Belfiore A. In IGF-1 receptor-deficient leiomyosarcoma cells autocrine IGF-2 induces cell invasion and protection from apoptosis via the insulin receptor isoform A. Oncogene 2002;21:8240–50.
41. Frasca F, Pandini G, Scalia P, et al. Insulin receptor isoform A, a newly recognized, high-affinity insulin-like growth factor 2 receptor in fetal and cancer cells. Mol Cell Biol 1999;19:3278–88.
42. Pandini G, Vigneri R, Costantini A, et al. Insulin and insulin-like growth factor-1 (IGF-1) receptor overexpression in breast cancers leads to insulin/IGF-1 hybrid receptor overexpression: evidence for a second mechanism of IGF-1 signaling. Clin Cancer Res 1999;5:1935–44.
43. Pandini G, Frasca F, Mineo R, Sciacca L, Vigneri R, Belfiore A. Insulin and insulin-like growth factor 1 hybrid receptors have different biological characteristics depending on the insulin receptor isoform involved. J Biol Chem 2002;277:39684–95.
44. Denley A, Carroll JM, Brierley GV, et al. Differential activation of insulin receptor substrates 1 and 2 by insulin-like growth factor-activated insulin receptors. Mol Cell Biol 2007;27:3569–77.
45. O'Reilly KE, Rojo F, She QB, et al. mTOR inhibition induces upstream receptor tyrosine kinase signaling and activates Akt. Cancer Res 2006;66:1500–8.
46. Crouthamel MC, Kahana JA, Korenchuk S, et al. Mechanism and management of AKT inhibitor-induced hyperglycemia. Clin Cancer Res 2009;15:217–25.
47. Garcia-Echeverria C, Pearson MA, Marti A, et al. *In vivo* antitumor activity of NVP-AEW541—a novel, potent, and selective inhibitor of the IGF-1R kinase. Cancer Cell 2004;5:231–9.
48. Okamoto K, Morison IM, Taniguchi T, Reeve AE. Epigenetic changes at the insulin-like growth factor 2/H19 locus in developing kidney is an early event in Wilms tumorigenesis. Proc Natl Acad Sci U S A 1997;94:5367–71.
49. Tarn C, Rink L, Merkel E, et al. Insulin-like growth factor 1 receptor is a potential therapeutic target for gastrointestinal stromal tumors. Proc Natl Acad Sci U S A 2008;105:8387–92.
50. Lakshmikuttyamma A, Pastural E, Takahashi N, et al. Bcr-Abl induces autocrine IGF-1 signaling. Oncogene 2008;27:3831–44.